Journal of *Marine Science and Engineering*

MDPI

Article

Prior-Guided Objective Detection and a 1993–2025 Monthly Record of the Northwest Atlantic Shelf-Slope Front

Shiliang Shan [1,2,*], Francois Rivest [3] and Blair Greenan [4]

[1] Department of Physics and Space Science, Royal Military College of Canada, Kingston, ON K7K 7B4, Canada
[2] Department of Civil Engineering, Queen's University, Kingston, ON K7L 3N6, Canada
[3] Department of Mathematics and Computer Science, Royal Military College of Canada, Kingston, ON K7K 7B4, Canada; francois.rivest@rmc.ca
[4] Bedford Institute of Oceanography, Fisheries and Oceans Canada, Dartmouth, NS B2Y 4A2, Canada; blair.greenan@dfo-mpo.gc.ca
* Correspondence: shiliang.shan@rmc.ca

Abstract

The Northwest Atlantic Shelf-Slope Front (SSF) separates colder, fresher shelf water from warmer, saltier slope water and influences shelf-slope exchange, coastal ocean variability, and ecosystem conditions. Fisheries and Oceans Canada's Atlantic Zone Monitoring Program (AZMP) maintained an analyst-derived monthly SSF position dataset beginning in 1973, but routine production ended after 2017. We developed a prior-guided objective sea surface temperature gradient peak detector to provide a reproducible ARMOR3D-based extension of this record. At integer longitudes from 75° W to 50° W, the detector identifies local maxima of the poleward cooling gradient and ranks them using peak prominence and distance from a seasonally adjusted shelf-break prior. Fivefold blocked cross-validation over 1993–2017 selected equal thermal prominence and geographic weighting. Across 6950 out-of-fold comparisons, bias was 0.095° latitude, root mean square error was 0.497°, median absolute error was 0.236°, and 75.7% of positions were within 0.50° of the AZMP-derived SSF. Seasonal peak timing differed by 0.13–0.35 months among the western, central, and eastern regions, and annual correlations were 0.89, 0.74, and 0.69, respectively. However, Peak SSF annual standard deviations were only 49–56% of the AZMP values, so the two records are not directly homogeneous in variability amplitude. The 2018–2025 portion is an ARMOR3D-based extension that has not been independently validated. It reveals regional contrasts rather than a persistent domain-wide displacement. The 1993–2025 Peak SSF dataset provides a reproducible, updateable benchmark for frontal monitoring, shelf-slope exchange studies, ecosystem analysis, and ocean model evaluation.

Keywords: Shelf-Slope Front; sea surface temperature; prior-guided objective detection; ARMOR3D; Gulf Stream; Northwest Atlantic

Check for updates

Academic Editor: Alberto Ribotti

Received: 20 August 2026
Revised: 16 October 2026
Accepted: 19 October 2026
Published: 26 October 2026

Copyright: © 2026 by the authors. Licensee MDPI, Basel, Switzerland. This article is an open access article distributed under the terms and conditions of the Creative Commons Attribution (CC BY) license.

1. Introduction

Ocean fronts are narrow regions of enhanced horizontal density gradients that are often accompanied by jets, convergent or divergent flow, and elevated vertical exchange. They organize the distribution and transport of physical and biogeochemical properties and shape marine ecosystems over broad spatial scales [1]. Along continental margins worldwide, shelf-break fronts form where shelf and open-ocean water masses meet. Their position and strength respond to bathymetry, buoyancy forcing, winds, and adjacent currents. Exchange across these fronts redistributes heat, freshwater, nutrients, plankton,

and other materials [2]. The Northwest Atlantic is a particularly dynamic example because its shelf-break front lies immediately north of the energetic Gulf Stream system (Figure 1).

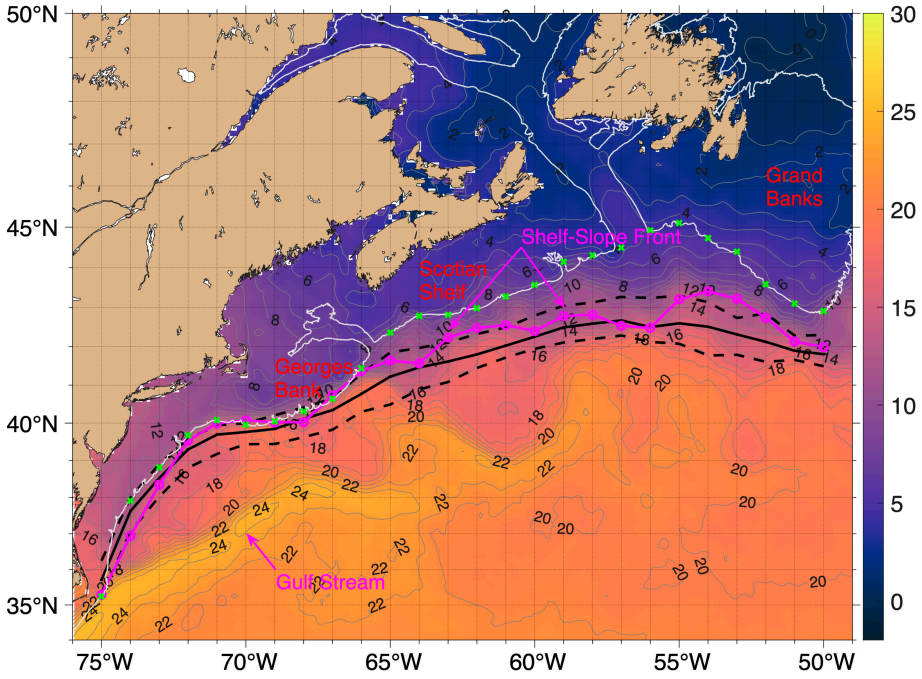


Figure 1. Monthly mean ARMOR3D sea surface temperature (SST, °C) for May 1993, showing the Shelf-Slope Front (SSF) and Gulf Stream. Color shading and dark gray contours show the SST field and isotherms. The magenta line with circles marks the analyst-derived AZMP SSF position for May 1993. The solid black line shows the May climatological mean SSF for 1993 to 2017, and the dashed black lines show ±1 standard deviation. The dark gray line denotes the 200 m isobath, and the green crosses mark its intersections with the sampled integer longitudes. At 57° W, near the entrance to the Laurentian Channel, the 450 m isobath is used instead to account for the deep channel bathymetry and maintain continuity in the shelf-break position between adjacent longitudes.

Early studies referred to this Northwest Atlantic boundary as the shelf water/slope water front or the shelf/slope front [3]. It is now commonly termed the Shelf-Slope Front (SSF) [4]. The SSF follows the continental shelf break from Cape Hatteras to the Grand Banks and forms the landward boundary of the Slope Sea (Figure 1). Csanady and Hamilton [5] described the Slope Sea as approximately 1600 km long and 200 km wide, with shelf water and Labrador-origin water on its landward side and Gulf Stream water on its seaward side. Hydrographic studies by Gatien [6] and Hinrichsen and Tomczak [7] distinguish warm slope water and Labrador-influenced slope water, whose distributions vary with the Labrador Current and the Gulf Stream. Houghton et al. [8] and Gawarkiewicz et al. [9] documented cross-shelf mixing and intrusions that transfer heat, salt, nutrients, and other tracers between these water masses. The SSF marks a dynamically active frontal zone and provides a surface indicator of the hydrographic state of the Northwest Atlantic margin.

Because the SSF often has a clear surface thermal expression, it has long been monitored with infrared SST imagery. Chamberlin [10] and Bisagni et al. [4] showed that, under sufficiently clear conditions, satellite observations provide synoptic views of the front and its seasonal evolution. Analysts at Fisheries and Oceans Canada interpreted SST charts produced by US government agencies and digitized SSF latitude at fixed longitudes from Cape Hatteras at 75° W to the Grand Banks at 50° W [11]. The resulting dataset was later maintained through the Atlantic Zone Monitoring Program (AZMP). Figure 1 shows the analyst-derived SSF for May 1993 together with its climatological path, and the SSF and the Gulf Stream North Wall are clearly visible, with pronounced Gulf Stream meanders and

mesoscale structure in the Slope Sea between them. Drinkwater and Bugden [12], Bisagni et al. [4], and Peterson et al. [13] used the AZMP SSF dataset to examine its mean path, seasonal migration, and links between frontal displacement, shelf and slope temperatures, and North Atlantic wind forcing. The AZMP dataset therefore provides an important long-term record for quantifying SSF variability and examining its relationships with shelf and slope hydrography and atmospheric forcing.

Routine production of the AZMP SSF dataset ended in 2017, leaving no ongoing extension of this long-term climate dataset. Manual chart interpretation is labor-intensive, difficult to reproduce exactly, and sensitive to analyst judgment when a meridional SST profile contains several plausible gradients. An objective, reproducible algorithmic extension avoids these limitations. Here, "objective" refers to the consistent application of explicit, quantitative, fixed rules after calibration, rather than independence from the historical AZMP observations used to calibrate the prior. The method must also preserve the historical feature definition of the AZMP SSF dataset while keeping the evidence and selection rule for each position explicit and reproducible.

Continuing the AZMP SSF dataset requires both detection of thermal fronts and identification of the SSF among them. General objective front-mapping algorithms locate thermal boundaries anywhere in an SST image. Common approaches include histogram-based contextual edge detection, local gradient mapping, and repeated front detection to construct occurrence maps, climatologies, and atlases. Cayula and Cornillon [14] developed a contextual edge detector for SST imagery, Ullman and Cornillon [15] applied objective front detection to the northeast United States shelf, Belkin and O'Reilly [16] detected fronts in both SST and chlorophyll imagery, and Cyr and Larouche [17] compiled a thermal-front atlas for Canadian coastal waters. Target-specific methods instead locate one named front and use approximate position, orientation, or continuity to stabilize the estimate, as in Shaw and Vennell [18] and Hopkins et al. [19]. Evaluation must distinguish the availability of a detectable gradient near the reference position from correct assignment of the SSF identity when several candidates are present [20].

Feature identity is especially challenging in the Northwest Atlantic because one meridional section can cross several physically distinct thermal fronts. Chamberlin [10], Gawarkiewicz et al. [9], and Bisagni et al. [21] show that a profile may contain the SSF, the Gulf Stream North Wall, warm-core ring edges, shelf-water streamers, and other mesoscale gradients. A single sigmoid or error-function fit to the full profile can therefore select the wrong boundary or combine separate transitions [22,23]. This limitation matters because the Gulf Stream North Wall is a thermal boundary that does not necessarily coincide with the Gulf Stream velocity core and remains distinct from the SSF [24]. Chi et al. [24] and McWilliams et al. [25] further show that mesoscale eddies between the two fronts and seasonal changes in the surface temperature gradient complicate a single-transition fit. These conditions favor retaining several SST gradient peaks before applying physical selection criteria.

Because gradient strength alone cannot identify the SSF, we separate thermal detection from feature assignment with a geophysically informed statistical method. We implement a two-stage Peak SSF detector. Candidate SST fronts are first detected objectively as local maxima of the poleward SST gradient, after which the SSF is identified from these candidates using peak prominence, an AZMP-calibrated shelf-break prior, and regional screening criteria. The prior guides feature assignment but does not prescribe the selected position, because every selected location must coincide with an observed SST gradient peak. Candidate latitude, prominence, score components, rank, and screening flags are retained so that each selected position can be traced to the observed gradient and the geographic evidence used in its selection.

This study tests whether local SST gradient evidence and shelf-break context can reproduce the historical AZMP definition without prescribing the frontal path. The objectives are to (1) generate SSF candidates from local SST gradient peaks in a monthly gridded ocean observational analysis, (2) rank the candidates with a seasonally adjusted shelf-break context and regional screening criteria, (3) evaluate agreement with the AZMP SSF dataset through blocked cross-validation, and (4) produce an ARMOR3D-based extension of monthly SSF monitoring through 2025. Section 2 describes the data and methods. Section 3 evaluates the detector and presents seasonal and interannual variability. Section 4 discusses physical interpretation, methodological strengths and limitations, applications, and future development. Section 5 presents the main conclusions.

2. Materials and Methods

2.1. Historical Analyst-Derived SSF Reference Dataset

We used the analyst-derived AZMP SSF dataset as the reference for calibration and evaluation. Drinkwater et al. [11] established its spatial framework by digitizing monthly frontal latitude at integer longitudes from 75° W to 50° W from satellite SST analyses beginning in 1973. Bisagni et al. [4] subsequently documented and reanalyzed the dataset. It was maintained through AZMP, and routine production ended after 2017. The dataset represents the surface thermal frontal zone between cooler, fresher shelf water and warmer, saltier slope water rather than a generic SST gradient maximum. Its historical definition follows the shelf-break-aligned surface thermal transition between shelf and slope waters. The 1993–2017 portion overlaps the ARMOR3D record and provides the reference observations used to calibrate and evaluate the prior-guided detector.

2.2. Modern Gridded ARMOR3D SST Dataset

A consistent extension requires monthly SST fields that span the full study domain from the start of the modern satellite altimetry era in 1993. We used monthly surface ARMOR3D SST from January 1993 through December 2025. ARMOR3D is a gap-free Level 4 observational analysis on a regular 1/8° grid that combines satellite SST and altimetry with in situ temperature and salinity profiles through empirical relationships and optimal interpolation, as described by Guinehut et al. [26], Mulet et al. [27], and the Copernicus Marine Service [28]. ARMOR3D uses the Operational Sea Surface Temperature and Sea Ice Analysis (OSTIA) as its upstream SST input, which combines infrared and microwave satellite observations with in situ temperature measurements. This observation-constrained dataset reduces cloud-related gaps while retaining frontal structure represented by the contributing observations.

ARMOR3D has demonstrated the frontal resolution needed for target-specific feature identification in the Northwest Atlantic. Chi et al. [24] used the 200 m ARMOR3D temperature field to distinguish the Gulf Stream from the Gulf Stream North Wall because ARMOR3D showed closer agreement with observations and resolved downstream longitudinal structure that was absent from the lower-resolution EN4 monthly analysis derived from in situ hydrographic profiles. This evidence indicates that ARMOR3D retains the spatial structure needed to distinguish nearby frontal features. Its three-dimensional (3D) temperature and salinity fields also provide a basis for future investigation of subsurface SSF structure and variability. Copernicus distributes ARMOR3D as a consistently reprocessed multi-year analysis with a near-real-time continuation, so the same detector can be applied as new monthly fields become available. Its frontal resolution, 3D structure, and continuing availability therefore make ARMOR3D suitable for a reproducible extension of the SSF dataset.

The analysis domain was 32° N–46° N and 75° W–50° W. It spans the northern Sargasso Sea and Gulf Stream to the south, the Slope Sea, the continental slope and shelf break, and the adjacent Northwest Atlantic shelf from Cape Hatteras to the Grand Banks. For each month, we extracted one meridional SST profile at each of 26 integer longitudes. We denote SST as $T(\phi, \lambda, t)$, where ϕ is latitude, λ is longitude, and t is month. The longitude grid resolution was 1°, and the native ARMOR3D latitude grid resolution was 0.125°.

January 1993 through December 2017 is the common period for ARMOR3D and the AZMP SSF dataset. AZMP positions were available in 6950 of the 7800 possible longitude-month cells (89.1%). Eight of the 300 months contained no AZMP positions, and most remaining gaps occurred in contiguous central or eastern sectors rather than as isolated cells. These spatially uneven gaps resulted from cloud cover, weak surface thermal expression, and incomplete source chart coverage [4]. Specifically, the dominant contiguous gap occurred at 54° W–50° W from May 1996 through April 2005, when the source chart product did not extend east of 55° W [21].

2.3. SST Gradient Candidate Generation

The Peak SSF detector has two stages. Candidate generation identifies local maxima in the poleward SST gradient, so every candidate coincides with a gradient peak present in the monthly SST profile. Candidate ranking combines normalized peak prominence with distance from a seasonally adjusted shelf-break prior.

Before any geographic preference was applied, candidate generation retained all local poleward cooling structures that could represent the SSF. For each longitude and month, the SST profile was transformed into the poleward cooling gradient as follows:

$$G(\phi, \lambda, t) = \max\left[0, -\frac{\partial T(\phi, \lambda, t)}{\partial \phi}\right] \quad (1)$$

where G is expressed in °C per degree latitude. Equation (1) retains locations where SST decreases toward the north and sets gradients of the opposite sign to zero. This sign convention represents the typical transition from warm slope water to colder shelf water. Retaining local maxima allows several observed gradients to remain available within one profile. Local maxima were identified with the findpeaks function in MATLAB R2025b using a minimum separation of 0.25° latitude, equivalent to two native ARMOR3D latitude grid cells.

To accommodate seasonal and regional changes in gradient strength, the minimum accepted prominence was $P_{\min} = \max(P_{\text{floor}}, k_{\text{Prom}}\, s_G)$. Here s_G is the normal-consistent median absolute deviation scale of G. The fixed lower limit P_{floor} was 0.01 °C per degree latitude. The tuning parameter k_{Prom} controls candidate generation sensitivity in MATLAB findpeaks. A smaller value lowers the prominence threshold and retains more peaks, including weaker gradients, whereas a larger value retains fewer, more prominent peaks and can exclude weak SSF expressions. The value of k_{Prom} was estimated by blocked cross-validation. For every candidate, the algorithm retained latitude, gradient value, width, prominence, SST, and water depth.

2.4. Seasonal Shelf-Break Prior, Candidate Ranking, and Regional Screening

A longitude-dependent geographic prior, $\phi_{\text{prior}}(\lambda, \text{m})$, represented the expected SSF latitude based on its offset from the shelf break:

$$\phi_{\text{prior}}(\lambda, \text{m}) = \phi_{\text{SB200}}(\lambda) + \mu_\lambda(\lambda) + \gamma_{\text{m}} \quad (2)$$

In Equation (2), ϕ_{prior} is the prior center latitude at longitude λ and month m, ϕ_{SB200} is the latitude of the local 200 m shelf break, μ_λ is the fitted longitude-dependent mean offset,

and γ_m is the zero-mean displacement for month m. Shelf-break latitudes were derived from GEBCO 2026 bathymetry and are shown by green crosses in Figure 1 [29].

The AZMP climatology places the SSF generally within about 50 km seaward of the 200 m contour from Cape Hatteras to Georges Bank, but the offset increases to about 250 km near 55° W east of the Laurentian Channel [4]. We modeled this offset with a continuous piecewise linear function with fixed knots at 65° W and 55° W. The four coefficients were estimated by Huber iteratively reweighted least squares with a tuning constant of 1.345 to limit the influence of large departures [30].

Monthly displacements were estimated from the longitude model residuals and centered to sum to zero. The longitude term represents the annual mean path, and the monthly term represents the documented seasonal migration [4,12,13]. The prior guides candidate ranking but does not prescribe the selected latitude because every Peak SSF position must remain a local SST gradient peak.

The candidate ranking score, Q_c, is defined by Equation (3) as the combination of a thermal prominence reward and a geographic reward. The thermal term increases with candidate prominence P_c relative to P_{scale}, defined as the larger of 0.10 °C per degree latitude and the 75th percentile of positive training prominences. The geographic term decreases with distance from the seasonal prior center, with the spread σ_{score} equal to the larger of 0.20° and the standard deviation of training residuals about Equation (2).

$$Q_c = (1 - \alpha_{SB})\left[1 - \exp\left(-\frac{P_c}{P_{scale}}\right)\right] + \alpha_{SB}\exp\left[-\frac{1}{2}\left(\frac{\phi_c - \phi_{prior}(\lambda, m)}{\sigma_{score}}\right)^2\right] \quad (3)$$

In Equation (3), α_{SB} is the relative weight assigned to geographic evidence. Because both rewards are scaled from zero to one, $\alpha_{SB} = 0$ uses prominence alone and $\alpha_{SB} = 1$ uses the prior alone. A value of $\alpha_{SB} = 0.5$ gives equal weight. This value was selected by blocked cross-validation, and candidates were ranked by decreasing Q_c.

Two regional screens were applied after ranking. From 74° W to 71° W, where strong Gulf Stream North Wall gradients can compete with the SSF, the western screen was introduced to reject occasional selections of the Gulf Stream North Wall that produced unrealistically large departures. At each longitude, the standard deviation (σ) was estimated robustly from the central 80% of the AZMP training residuals using the corresponding standard normal 10th-to-90th percentile span, which reduces sensitivity of the estimated spread to extreme residuals. Cutoffs of 2–4σ were tested. The 3σ cutoff yielded the lowest pooled out-of-fold RMSE and was therefore selected.

The eastern SST consistency screen addressed ambiguity caused by weak SSF gradients and nearby mesoscale structure. Because the detector treats each longitude independently, competing peaks can produce abrupt, physically implausible along-front SST jumps. From 65° W to 50° W, a candidate remained eligible when its SST was within 2.0 °C of the monthly median SST of the preliminary highest-ranked candidates. This ARMOR3D-derived reference allows seasonal, interannual, and along-front temperature variability while excluding candidates on a distinctly different water mass boundary, without using AZMP temperature [12]. The 2.0 °C tolerance was selected from a sensitivity test using thresholds of 1.0, 1.5, 2.0, and 2.5 °C, as a balance between allowing realistic along-front SST variability and excluding abrupt, thermally inconsistent candidate selections without making the screen overly restrictive.

The Peak SSF was the highest-ranked candidate that passed all applicable screens. Its latitude was refined with a three-point parabolic fit to the local maximum of G. The adjustment was limited to 0.0625°, half of the native ARMOR3D latitude spacing, and SST and depth were interpolated to the refined position. Candidate positions, score components, ranks, and screening flags were retained for traceability.

2.5. Parameter Calibration, Validation, and Dataset Construction

The detector has two tuning parameters with different roles. k_{Prom} controls candidate generation sensitivity through the prominence threshold in Equation (1), while α_{SB} controls the relative influence of the shelf-break prior in the candidate ranking score in Equation (3). Both parameters were tuned using fivefold blocked cross-validation over 1993–2017. Each validation block contained 5 consecutive years, and the remaining 20 years formed the training set. Within every training set, the longitude model, month displacements, score scales, and western screening scale were re-estimated before the omitted years were evaluated. This design ensured that each validation block was evaluated with a detector fitted only to the other 20 years. AZMP positions from the withheld years were not used to fit the prior, set the score scales, or define the western screening scale.

Parameter tuning used a coarse-to-fine grid search. The initial grids were k_{Prom} = {0.50, 1.00, 1.50} and α_{SB} = {0, 0.50, 1.00}. The next grid was centered on the stage-best pair with the spacing reduced by a factor of 2. Combinations satisfying mean absolute fold bias $\leq 0.125^{\circ}$, equal to the native ARMOR3D latitude grid resolution, were ranked by mean fold RMSE. The incumbent best pair was replaced only if RMSE improved by at least $\max(0.001^{\circ}, 0.10 s_{\mathrm{RMSE}})$, where s_{RMSE} is the standard deviation of RMSE among folds. Otherwise, refinement stopped, and the incumbent best pair was retained as the final tuned parameters. The resulting tuned parameters are reported in Section 3.1.

During parameter tuning, mean fold RMSE was minimized subject to the mean absolute fold bias constraint described above. Detector performance was then summarized with metrics that distinguish systematic displacement, overall positional error, a robust measure of typical positional error, and the availability of a nearby gradient candidate. Signed positional error was Peak SSF latitude minus AZMP SSF latitude, so positive values indicate a northward Peak SSF estimate. Bias measures systematic meridional displacement. RMSE gives greater weight to large mismatches, while mean absolute error summarizes average positional differences and median absolute error provides a robust measure of typical positional error because it is less sensitive to large mismatches. Percentages within 0.25° and 0.50° describe agreement within two and four native ARMOR3D latitude grid cells. Candidate recall is the percentage of AZMP positions for which at least one generated gradient peak lies within the stated tolerance, regardless of which candidate is selected. Comparing candidate recall with selected-position accuracy distinguishes limitations in peak generation from limitations in assigning SSF identity.

To separate independent performance evaluation from construction of the complete Peak SSF dataset, we used two overlap assessments. Blocked out-of-fold metrics were used to evaluate predictions for years excluded from all prior and score-scale fitting. After parameter selection, the shelf-break prior and scoring scales were re-estimated from all available AZMP observations from 1993 through 2017, and the fixed detector was applied to all 396 months from January 1993 through December 2025 at the 26 integer longitudes from 75° W to 50° W. Full-overlap metrics then describe agreement between the final 1993–2017 Peak SSF dataset and the available AZMP positions. The monthly AZMP and Peak SSF datasets are provided in the Supplementary Materials and analyzed in Section 3.

3. Results

3.1. Evaluation of the Peak SSF Against the AZMP SSF Dataset

This section first reports the tuned parameter values, then illustrates candidate selection using the May 1993 conditions shown in Figure 1, and finally evaluates pointwise and longitude-time agreement over 1993–2017 before examining seasonal and interannual variability.

Following the coarse-to-fine tuning procedure described in Section 2.5, the search first identified the best coarse-grid parameter pair and then evaluated a locally refined grid. The best coarse-grid pair was $k_{\mathrm{Prom}} = 1.00$ and $\alpha_{\mathrm{SB}} = 0.50$. The refinement factor was 2, so the fine grid was centered on the coarse-stage optimum and evaluated $k_{\mathrm{Prom}} = \{0.75, 1.00, 1.25\}$ and $\alpha_{\mathrm{SB}} = \{0.25, 0.50, 0.75\}$. Its RMSE improvement did not exceed the predefined cross-validation threshold, so the search stopped and the selected pair remained $k_{\mathrm{Prom}} = 1.00$ and $\alpha_{\mathrm{SB}} = 0.50$. The prominence multiplier therefore set the adaptive part of the threshold to one robust gradient scale, and the geographic weight assigned equal contributions to the normalized prominence and shelf-break prior terms. These values were fixed for producing the Peak SSF from 1993 to 2025.

May 1993 illustrates how the Peak SSF detector resolves a month with complex frontal structure (Figure 2). A pronounced Gulf Stream meander and several additional SST gradients produced multiple gradient peak candidates in many meridional profiles. At each longitude, rank 1 denotes the highest-scoring candidate according to Equation (3) with the selected $k_{\mathrm{Prom}} = 1.00$ and $\alpha_{\mathrm{SB}} = 0.50$, and the sequence of rank 1 candidates forms the cyan Peak SSF path. Despite the competing gradients, this path remained close to the magenta AZMP SSF from the Mid-Atlantic Bight to the Grand Banks. The example shows why retaining several observed peaks before assigning SSF identity is preferable to selecting the strongest gradient alone.

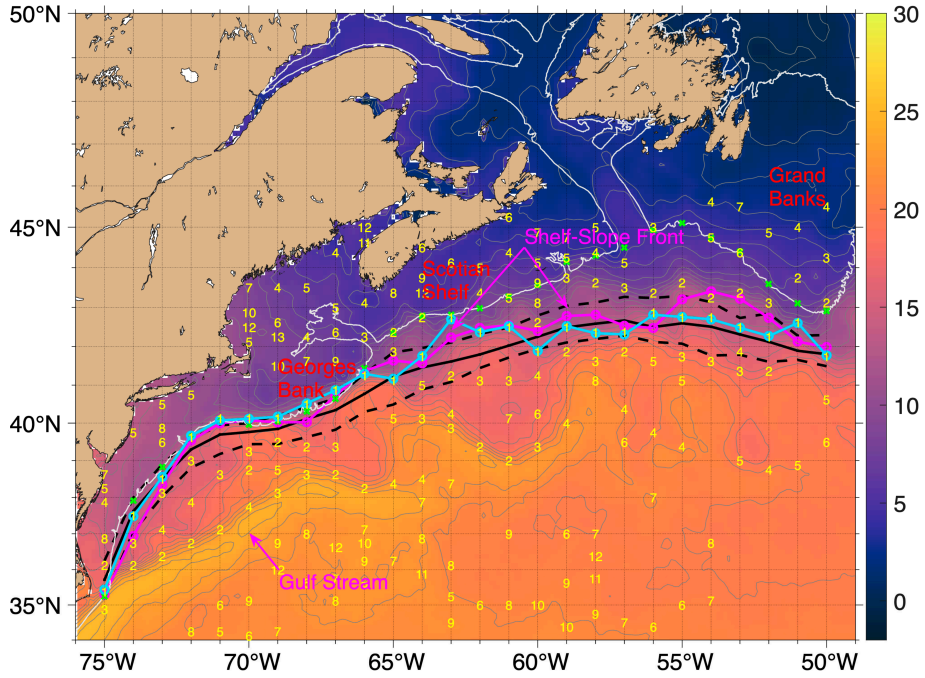


Figure 2. Same as Figure 1 with prior-guided Peak SSF positions overlaid as a cyan line. Numbers denote the ranks of candidate frontal peaks at each sampled longitude.

Blocked cross-validation showed that Peak SSF positions followed the AZMP latitude distribution with little systematic offset (Figure 3). Across 6950 out-of-fold comparisons, bias was +0.095°, RMSE was 0.497°, median absolute error was 0.236°, and 75.7% of positions were within 0.50°. The fold-mean RMSE was 0.495° with a standard error of 0.019°, indicating limited sensitivity to which the 5-year block was withheld. Regional pooled out-of-fold RMSE increased from 0.443° in the western sector to 0.524° in the central sector and 0.554° in the eastern sector; the eastern sector RMSE was approximately 25% higher than the western sector value. After the detector was refitted with all overlap observations, agreement remained nearly unchanged. Across all matched 1993–2017 positions, bias was

+0.097°, RMSE was 0.490°, mean absolute error was 0.347°, median absolute error was 0.232°, and 52.7% and 76.2% of positions were within 0.25° and 0.50°. The similarity of the two assessments shows that the final refit changed overlap agreement little, although only the out-of-fold metrics provide an independent assessment.

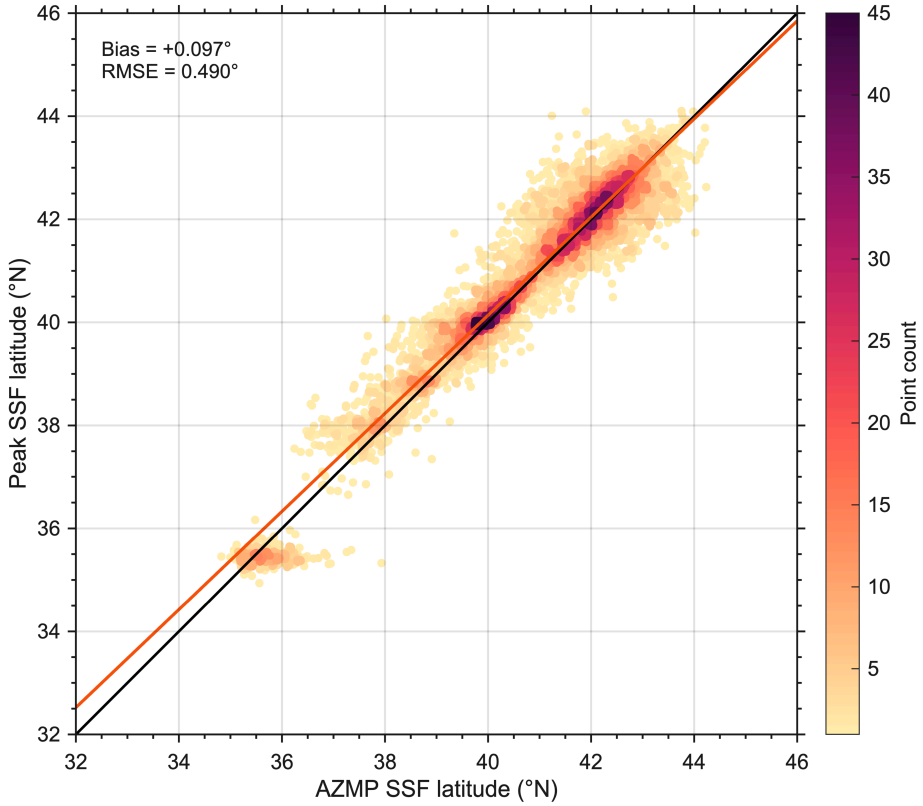


Figure 3. Scatter plot comparing prior-guided Peak SSF latitudes with AZMP SSF latitudes for paired monthly values from 1993 to 2017. The black line is the 1:1 line, the orange line is the least squares regression, and point color indicates local point count. Bias and root mean square error (RMSE) are shown in the upper left.

Across the 6950 out-of-fold comparisons, candidate recall was 68.7% within 0.25° and 94.1% within 0.50°, compared with selected-position accuracies of 52.3% and 75.7%, respectively. Thus, at the 0.50° tolerance, a plausible candidate was usually generated, and most remaining failures arose during the ranking and assignment of competing frontal features. Improvements should therefore focus on feature discrimination in candidate ranking rather than on lowering the peak-detection threshold.

The regional screening criteria altered a limited subset of preliminary selections and operated differently by region. At the selected 3σ threshold, the western position consistency screen changed 26 of 1584 selections from 74° W to 71° W (1.64%). Visual inspection confirmed that these corrections removed isolated misidentifications of the Gulf Stream North Wall while retaining plausible SSF variability. From 65° W eastward, the eastern SST consistency screen changed 861 of 6336 selections (13.59%). The western criterion therefore corrected rare large jumps, while the eastern criterion addressed more frequent competition among gradients with dissimilar temperatures associated with meanders and rings.

Figure 3 summarizes matched positions point by point, while Figure 4 shows how SSF anomalies, data gaps, and differences between the datasets vary with longitude and time. During 1993–2017, AZMP and Peak SSF anomalies show many of the same broad northward and southward bands, including the generally southward conditions of the mid-2000s and northward conditions of the early to mid-2010s described by Peterson et al. [13]. The

smaller anomaly magnitude of the Peak SSF may partly reflect the shelf-break prior, which favors candidates near historically common positions and can suppress large excursions. Regression slopes of Peak SSF anomaly against AZMP anomaly were 0.423, 0.408, and 0.384 in the western, central, and eastern regions, respectively. The below-one slopes confirm that Peak SSF captures broad variability but underestimates the magnitude of frontal excursions. This limitation is discussed further in Section 4.2. The Peak SSF panel also fills longitude-month cells where AZMP is missing and continues the monthly dataset through 2025. The following sections examine the seasonal and interannual variability represented in these fields.

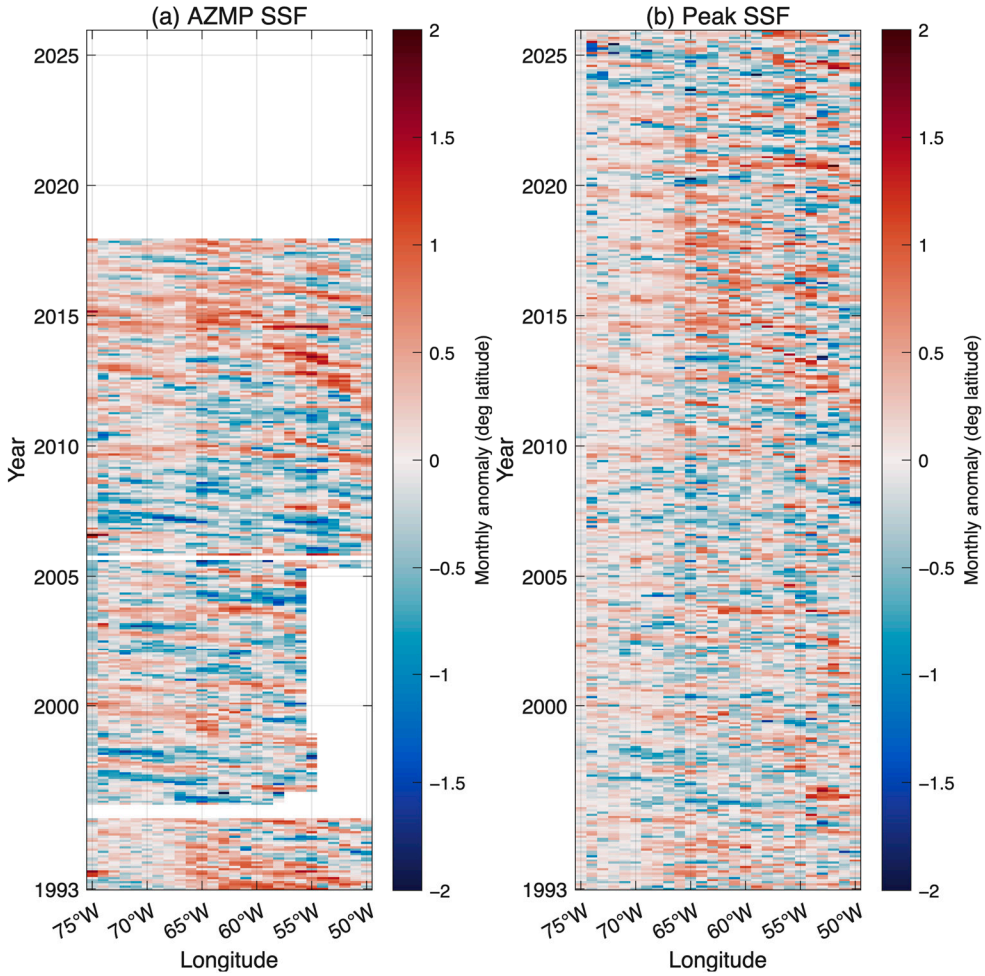


Figure 4. Time versus longitude diagrams of monthly SSF latitude anomalies for (**a**) the AZMP SSF and (**b**) the Peak SSF. Red indicates positive, northward anomalies, and blue indicates negative, southward anomalies. White areas denote missing data.

3.2. Seasonal Variability

Peak SSF monthly latitude anomalies during 1993–2017, calculated relative to the period mean at each longitude, showed a coherent annual cycle across most of the 75° W–50° W domain (Figure 5a). Positive anomalies occurred mainly from late summer through autumn, whereas negative anomalies were concentrated from late winter through spring. The annual harmonic placed the northward maximum in September in the western region (75° W–66° W), October in the central region (65° W–56° W), and August in the eastern region (55° W–50° W). The opposing southward maximum in these three regions occurred 6 months later in March, April, and February, respectively. The timing of

these meridional anomalies is consistent with the seaward winter and shoreward summer cycle reported by Bisagni et al. [4].

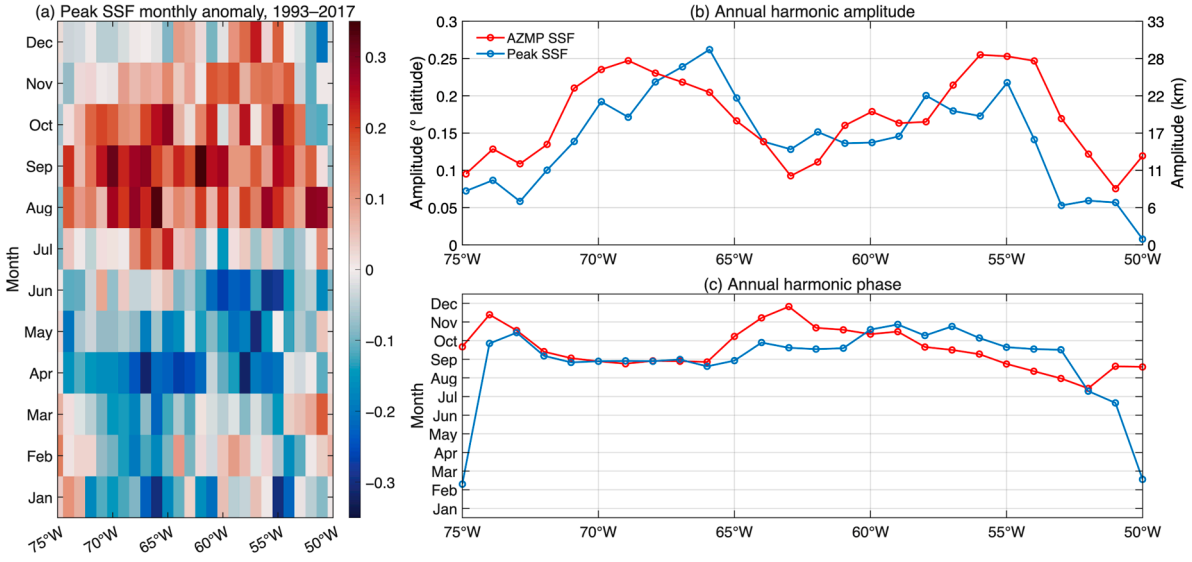


Figure 5. Seasonal variability of the SSF during 1993 to 2017. (**a**) Climatological monthly mean Peak SSF latitude anomalies by longitude; red and blue indicate northward and southward anomalies, respectively, with color-scale units in degrees latitude. (**b**) Annual harmonic amplitude at each longitude in degrees latitude (left axis) and kilometers (right axis). (**c**) Month of maximum northward displacement. The AZMP SSF is red, and the Peak SSF is blue in (**b**,**c**).

The seasonal amplitude averaged for each region showed strongest agreement between the AZMP and Peak in the central region, with a modest reduction in agreement in the west and a larger reduction in the east (Figure 5b). In the central region, AZMP and Peak SSF amplitudes were nearly identical at 0.169 ± 0.045° and 0.163 ± 0.026° (mean ± standard deviation, 18.8 and 18.1 km). The western amplitudes were 0.185 ± 0.056° for AZMP and 0.159 ± 0.071° for the Peak SSF, a difference of 0.026° or 2.9 km. The largest regional difference occurred in the east, where amplitude decreased from 0.169 ± 0.070° (18.7 km) to 0.096 ± 0.074° (10.7 km). Thus, the detector retained the broad seasonal cycle across the domain, but the magnitude became progressively more damped toward the eastern boundary.

The eastern amplitude maximum was only partly reproduced. AZMP amplitudes reached approximately 0.25° from 56° W to 54° W, corresponding to a fitted peak-to-peak excursion of about 56 km and agreeing with the approximately 50 km seasonal variability east of 58° W reported by Bisagni et al. [4]. The Peak SSF retained a local maximum of 0.223° (24.8 km) at 55° W but had substantially smaller amplitudes farther east. The detector therefore preserved the location of part of the eastern seasonal maximum but underestimated its full magnitude.

Seasonal phase agreed more closely than amplitude (Figure 5c). The circular mean month of maximum northward displacement was 9.40 for AZMP and 9.27 for the Peak SSF in the west, 10.37 and 10.02 in the central region, and 8.29 and 8.60 in the east. The regional differences were 0.13, 0.35, and 0.31 months. The Peak SSF also retained the later central maximum relative to the east, although the eastern phase became less spatially coherent where harmonic amplitude was small toward 50° W. Neither dataset showed the complete 180° east–west phase reversal reported for 1973–1992 by Bisagni et al. [4], partly because the present analysis uses meridional anomalies at fixed longitudes and a later period. The close phase agreement with AZMP should not be interpreted as a fully independent recovery of

seasonality, because the detector includes an AZMP-derived monthly displacement term. The sensitivity of amplitude and phase to this term is examined in Section 4.2.

3.3. Interannual Variability

Annual Peak SSF anomalies included coherent shifts across the full domain and opposing regional changes (Figure 6). The front was generally south of its mean during 2006–2008 and north during 2014–2015. The strongest coherence occurred in 2007–2008 and 2014–2015, when most longitudes shared the same anomaly sign. In contrast, 1996, 2010, and 2012 showed opposing anomalies among regions, indicating deformation of the frontal path rather than uniform translation. These patterns are consistent with the strong longitude dependence of SSF variability documented by Bisagni et al. [4] and Peterson et al. [13].

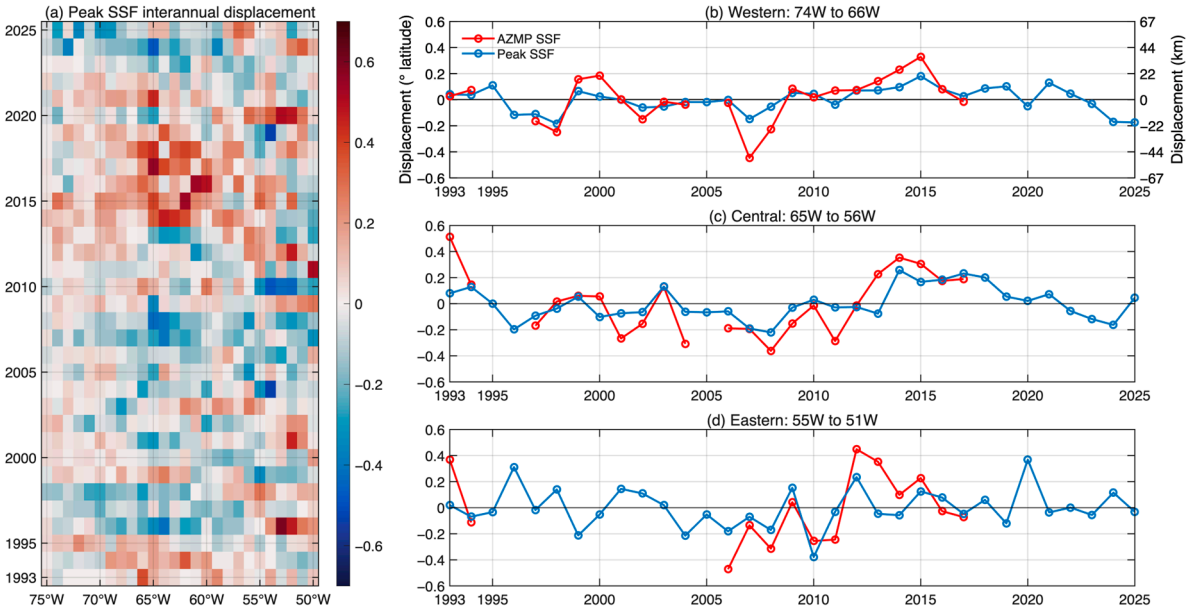


Figure 6. Interannual variability of the SSF. (**a**) Annual mean Peak SSF latitude anomalies by longitude from 1993 to 2025; red and blue indicate northward and southward anomalies, respectively, with color-scale units in degrees latitude. Panels (**b**–**d**) show regional mean anomalies for the western (74° W to 66° W), central (65° W to 56° W), and eastern (55° W to 51° W) sectors. The AZMP SSF is red, and the Peak SSF is blue. Positive and negative values denote northward and southward displacement, respectively; the right axis in (**b**) gives kilometers.

Agreement with AZMP decreased eastward. Based on 22 common years in the western and central regions and 14 common years in the eastern region, regional annual Pearson correlations were 0.89 (95% CI: 0.76–0.96; $p < 0.001$), 0.74 (95% CI: 0.47–0.89; $p < 0.001$), and 0.69 (95% CI: 0.25–0.89; $p = 0.007$), respectively. RMSE values were 11.4, 17.9, and 22.2 km, and anomaly signs matched in 86%, 82%, and 79% of common years. Mean paired differences between Peak SSF and AZMP were −0.1, +0.7, and −2.7 km. Peak SSF standard deviations were only 49–56% of the AZMP values, ranging from 9.4 to 17.2 km compared with 19.3 to 30.9 km. These results identify two separate limitations: anomaly magnitude is underestimated in all three regions, while year-to-year positional agreement with AZMP decreases toward the east.

The Peak SSF extends monthly frontal positions through 2025, 8 years beyond the endpoint of AZMP. Because no AZMP positions are available after 2017, these regional summaries describe the extension rather than an independent validation. During 2018–2025, regional anomalies frequently differed in sign (Figure 6). The central and western regions were northward in 2018, 2019, and 2021, but both shifted south in 2020 as the eastern

region reached a pronounced northward position. Southward displacement became more persistent in the west during 2023–2025, while the central and eastern regions continued to vary independently.

The extension is characterized by regional divergence rather than a sustained shift across the full domain. No northward or southward displacement persisted in all three regions, consistent with the longitude-dependent behavior observed during the overlap. Linear trends in the annual regional Peak SSF anomalies over 1993–2025 were weakly northward in the western, central, and eastern regions, 1.09, 2.70, and 0.97 km decade^{-1}, respectively, but were not statistically significant based on Newey–West autocorrelation-consistent tests (p = 0.697, 0.415, and 0.630, respectively). Because 8 years is short relative to documented interannual SSF variability [13], the post-2017 record represents recent regional conditions rather than a robust trend.

4. Discussion

4.1. Physical Interpretation of Seasonal and Interannual Variability

The Peak SSF captures the principal timing and regional pattern of both seasonal and interannual variability, supporting its use as an ARMOR3D-based monthly extension of the AZMP dataset. The late summer to autumn northward maximum and late winter to spring southward maximum agree with the broad annual migration described by Bisagni et al. [4]. Longitudinal structure near the Laurentian Channel and Grand Banks is also consistent with changes in shelf orientation, Labrador-origin water influence, and regional slope-water circulation described by Gatien [6], Drinkwater and Bugden [12], and Hinrichsen and Tomczak [7]. Model results further show that slope-water properties reflect the combined influences of the Gulf Stream, Labrador Current, and surface forcing [31]. A single domain-wide seasonal amplitude or phase would therefore obscure important regional structure.

Interannual anomalies likewise describe changes in shelf-slope geometry rather than displacement of one rigid line. Peterson et al. [13] linked historical SSF position to shelf and slope temperatures and to large-scale wind stress curl. Earlier work by Houghton et al. [8] and Csanady and Hamilton [5] documented exchange, mixing, and circulation across the Scotian Shelf and Slope Sea. Process studies in the Sable Gully further show that wind forcing, tide-topography interaction, and shelf-scale circulation jointly shape circulation and hydrography near the Scotian Shelf break [32]. A northward latitude anomaly generally places the warm, saline slope-water boundary closer to the shelf interior, whereas a southward anomaly extends colder, fresher shelf influence farther over the slope. Although SSF latitude is not a direct transport estimate, it identifies the moving boundary between shelf and slope waters and provides a spatial framework for interpreting heat and freshwater exchange when combined with salinity, velocity, and subsurface observations.

Opposite-sign anomalies among regions indicate deformation of the SSF path rather than uniform translation of the entire front. Years such as 1996, 2010, 2012, and 2020 show that one region can move north while another moves south. Longitudinally opposing changes also occur in the nearby Gulf Stream path, although the Gulf Stream and SSF remain distinct features, as shown by Chi et al. [24] and Wang et al. [33]. A full-domain average can therefore cancel physically meaningful changes in the western, central, and eastern regions. Regional time series should be the primary summaries for process studies, with a domain mean used when displacement is spatially coherent.

4.2. Methodological Strengths and Limitations

The Peak SSF detector combines elements of general front mapping and target-specific feature localization. General edge detectors are designed to locate every SST boundary in an image, which is valuable for describing frontal occurrence but does not identify which edge

is the SSF. This candidate generation concept follows established approaches described by Cayula and Cornillon [14], Ullman and Cornillon [15], Belkin and O'Reilly [16], and Cyr and Larouche [17]. A single-transition fit imposes the opposite constraint by assuming that one profile contains one dominant boundary, an assumption that is often violated in the Slope Sea. The Peak SSF detector instead retains multiple candidates from local SST gradients and then uses the AZMP-calibrated shelf-break prior to identify one named front. This feature assignment step follows the target-specific logic of Shaw and Vennell [18] and Hopkins et al. [19]. The method preserves direct SST gradient evidence at the selected latitude while making its geographic assumptions explicit. It also allows candidate recall and final positional accuracy to be evaluated separately, revealing whether errors arise during candidate generation or during assignment of SSF identity.

A single maximum gradient or full-profile transition can represent the SSF, the Gulf Stream North Wall, or a mesoscale edge, depending on longitude and month. This ambiguity is evident in the analyses of Watelet et al. [22] and Chi et al. [23,24]. The shelf-break prior and regional screening criteria provide feature identity without smoothing the selected path across longitude or time. As a result, unusual but observed local structure remains visible in the candidate diagnostics rather than being forced onto a continuous climatological path.

A four-case sensitivity experiment was conducted to examine the relative contributions of the SST gradient information, the spatial and temporal components of the shelf-break prior, and the regional screening criteria to agreement with AZMP. The peak-detection parameters were first selected for the full baseline method ($k_{\mathrm{Prom}} = 1.0$ and $\alpha_{\mathrm{SB}} = 0.5$) and were then held fixed in all remaining cases so that the differences reflected only the removal of individual method components. The four cases were: (1) the full baseline case with the longitude-dependent shelf-break offset, monthly displacement, and regional screens; (2) Case 1 with both regional screens disabled; (3) Case 2 with the monthly displacement also disabled; and (4) Case 3 with the longitude-dependent offset removed, leaving an unshifted 200-m shelf-break prior. Across all four cases, the SST gradient candidate set contained a peak within 0.25° and 0.50° of the AZMP position in 68.7% and 94.1% of comparisons, respectively, showing that the gradient field generally identifies a plausible front candidate. The full method achieved an out-of-fold RMSE of 0.497°, with 52.3% and 75.7% of detections within 0.25° and 0.50° of AZMP, respectively. The RMSE increased to 0.548° when the screens were removed and to 0.564° when the monthly displacement was also removed, but rose to 1.213° when the longitude-dependent offset was disabled. The corresponding bias increased to +0.800°, and the fractions within 0.25° and 0.50° fell to 32.2% and 46.8%, respectively. Thus, the longitude-dependent shelf-break prior provides the principal constraint for resolving competing gradient peaks, whereas the monthly displacement and regional screening provide smaller, incremental refinements.

The sensitivity experiment also allowed us to quantify how the seasonal prior affects the recovered amplitude and phase of the annual cycle. The monthly displacement term consists of one zero-mean value for each calendar month, applied uniformly across all longitudes. Removing it reduced the harmonic amplitude by 26% in the west, 55% in the central region, and 59% in the east. The western phase remained relatively stable, whereas the central and eastern phases became spatially less coherent. Thus, the common monthly term does not directly prescribe regional seasonal cycles; rather, it helps the detector track a consistent SST gradient band where multiple candidates occur. Although the term is not longitude-dependent, its interaction with the local SST gradient structure supports the recovery of longitude-varying amplitudes and phases. The recovered seasonal cycle is therefore partly prior-guided, particularly in the central and eastern regions.

Agreement with AZMP SSF must be interpreted in light of uncertainty in both datasets. AZMP is the best available representation of the historical analyst definition of SSF, but

it is not an error-free geophysical truth. When several thermal fronts coexist, analyst judgment introduces positional uncertainty in the selected boundary. The comparison is also not between equivalent source fields. AZMP positions were interpreted from available infrared SST charts, and cloud cover, weak surface thermal expression, and incomplete source chart coverage produced missing months and longitude sectors. The Peak SSF is instead estimated from monthly gridded ARMOR3D fields that can smooth or merge nearby transitions. In addition, both datasets identify the surface thermal expression of a 3D hydrographic front. Bisagni et al. [4] and Peterson et al. [13] show that this surface expression can weaken even when a subsurface boundary persists. Agreement therefore measures continuity with the historical definition rather than proof that either latitude is exact.

The main detector-specific limitation is reduced anomaly amplitude. Seasonal amplitude was especially weak east of 55° W, and regional annual standard deviations were only 49–56% of AZMP values. Monthly averaging and objective interpolation in ARMOR3D can weaken narrow gradients. The shelf-break prior also favors candidates near historically common positions, which can suppress large excursions even when their sign and timing are correct. To isolate sensitivity to geographic weighting, k_{Prom} was fixed at 1.0, both regional screens were disabled, and α_{SB} was varied from 0.25 to 1.00 in increments of 0.25. The pooled out-of-fold RMSE was lowest at α_{SB} = 0.50 (0.548°), compared with 0.701°, 0.560°, and 0.584° at α_{SB} = 0.25, 0.75, and 1.00, respectively. Regional (west/central/east) standard deviation ratios declined from 1.380/0.753/0.751 at α_{SB} = 0.25 to 0.276/0.241/0.211 at α_{SB} = 1.00, showing progressively stronger variance suppression as the prior weight increased. The regional correlations with AZMP were 0.685/0.851/0.814, 0.880/0.514/0.768, 0.787/0.066/0.700, and 0.640/−0.091/0.244 at α_{SB} = 0.25, 0.50, 0.75, and 1.00, respectively. As the prior weight increased, correlations remained relatively high in the western region but became weak or absent in the central region above 0.50 and in the eastern region above 0.75, indicating that excessive shelf-break weighting can prevent recovery of the sequence of northward and southward SSF shifts in the AZMP record. The high variability at α_{SB} = 0.25 was largely caused by occasional switches to the Gulf Stream North Wall or continental shelf gradients rather than realistic SSF excursions. The prior does not move a selected position toward its climatological center. Every final position remains a local SST gradient peak, so damping occurs indirectly through candidate ranking when several gradients compete. The Peak SSF record therefore reproduces the timing and direction of regional variability more reliably than its full magnitude and should be used cautiously for analyses of extreme displacement, regime shifts, or climate relationships. Reducing this damping while maintaining reliable front identification remains an important methodological challenge.

Because no analyst-derived AZMP positions are available after 2017, the 2018–2025 Peak SSF record represents an ARMOR3D-based extension rather than an independently validated continuation. Its temporal transferability is supported by blocked cross-validation over 1993–2017, including comparable performance for the latest withheld block, 2013–2017. The post-2017 positions are not extrapolated from the historical frontal trajectory. Each selected position must correspond to a local SST gradient peak in the ARMOR3D field, while the shelf-break prior only guides candidate ranking. Blocked cross-validation, however, cannot replace an independent post-2017 reference. Future validation could use blinded expert delineation of representative post-2017 months, supplemented where available by coincident hydrographic observations of the SSF.

4.3. Applications of the Extended SSF Dataset and Future Development

The Peak SSF dataset provides a reproducible basis for ongoing frontal monitoring. Copernicus distributes ARMOR3D as a multi-year reprocessed analysis with a near-

real-time continuation [28]. As additional observations are processed, later fields can be analyzed with the fixed detector, preserving the method definition across updates. The 1993–2025 dataset also provides historical context for individual events and regional anomalies. Efforts will be made to integrate the Peak SSF record into the Atlantic Zone Monitoring Program and extend it periodically as part of the AZMP data products.

The same detector can be applied to regional model SST fields to evaluate mean SSF path, seasonal phase and amplitude, and regional interannual variability. High-resolution Northwest Atlantic circulation systems such as CIOPS-East [34] and DalROMS-NWA12 [35] are suitable applications because they represent shelf circulation, slope-water pathways, and mesoscale structure. The SSF is a dynamically important hydrographic boundary for cross-shelf exchange and the connection between coastal and open-ocean waters [2]. A model can reproduce broad temperature or sea-level statistics while placing this boundary incorrectly and therefore misrepresenting pathways of heat, freshwater, nutrients, and other tracers. The Peak SSF benchmark complements conventional temperature, current, and sea-level metrics, including the sea-level skewness diagnostic of Thompson and Demirov [36], by testing whether the model places the correct Shelf-Slope Front.

Beyond physical monitoring and ocean model evaluation, the Peak SSF dataset can provide environmental context for fisheries and ecosystem studies. Ocean fronts organize water masses, transport pathways, and biological distributions over broad spatial scales [1]. In the Northwest Atlantic, interactions between Gulf Stream warm-core rings and the outer shelf have been related to longfin squid relative abundance [21]. The longitude-resolved SSF positions can therefore be combined with fisheries surveys [21], plankton observations and ocean color fields [1,16], and animal tracking [37] to test whether biological distributions covary with frontal latitude, regional deformation, or distance from the SSF.

These monitoring, model evaluation, and ecosystem applications also motivate further development of the detector. Future work should first add multivariate evidence while retaining the present candidate diagnostics. Salinity, density, subsurface temperature, sea surface height, and eddy information could help distinguish the SSF from warm-core ring edges and other mesoscale gradients when SST contrast is weak. Multivariate studies by Zhang and Partida [38] and Chen et al. [39] illustrate the value of combining hydrographic and dynamical evidence for shelf-ocean exchange. A supervised probabilistic candidate ranker is the most direct machine learning extension because each AZMP longitude-month case supplies one reference position and several competing candidates. Learning-to-rank methods could use prominence, width, SST, depth, shelf-break distance, and neighboring consistency [40]. Validation would still require blocked temporal and regional designs because nearby observations are dependent [41]. A U-Net could eventually learn a two-dimensional frontal probability field, but that approach would require dense expert-labeled frontal paths rather than the present monthly positions at fixed longitudes [42]. The current detector therefore provides a physically interpretable benchmark for determining whether a learned model reduces positional error while preserving seasonal amplitude, interannual variance, and plausible extremes.

5. Conclusions

We developed a prior-guided objective Peak SSF detector to extend the analyst-derived AZMP Shelf-Slope Front record with monthly ARMOR3D SST. The method objectively detects local maxima in the poleward SST gradient and then identifies the SSF using peak prominence, an AZMP-calibrated seasonally adjusted shelf-break prior, and regional screening criteria. Objective denotes the consistent application of explicit, fixed rules after calibration rather than independence from the AZMP reference. This two-stage design

addresses the central problem of assigning SSF identity when one meridional profile contains several physically distinct thermal fronts.

Blocked cross-validation demonstrated useful continuity with the AZMP-defined SSF. Across 6950 out-of-fold comparisons, bias was 0.095°, RMSE was 0.497°, median absolute error was 0.236°, and 75.7% of positions were within 0.50°. A gradient candidate occurred within 0.25° and 0.50° in 68.7% and 94.1% of cases, respectively, showing that the remaining large discrepancies mainly reflect ranking among competing gradients.

The Peak SSF recovered seasonal phase and the sign of many annual anomalies but underestimated variability. Seasonal phase differed from AZMP by only 0.13–0.33 months across the three regions, while annual correlations were 0.89, 0.74, and 0.69 from west to east. Regional annual standard deviations were only 49–56% of the AZMP values, and anomaly-regression slopes were 0.423, 0.408, and 0.384. The Peak SSF and AZMP records therefore should not be treated as directly homogeneous in variability amplitude. Preserving anomaly magnitude while maintaining reliable feature identity is the main challenge for further method development.

Application through 2025 provides an 8-year ARMOR3D-based extension of reproducible monthly SSF monitoring and reveals strong regional contrasts rather than one common trend. Because no analyst-derived AZMP positions are available after 2017, the 2018–2025 extension has not been independently validated and, therefore, should not be interpreted as a validated continuation of the historical record. With this limitation and the reduced variability amplitude in mind, the historical AZMP and Peak SSF records provide complementary context for studies of seasonal and interannual variability, shelf-slope exchange, coastal heat and freshwater pathways, and ocean model evaluation. Future multivariate and supervised ranking methods should be evaluated against this transparent benchmark and should improve anomaly magnitude without sacrificing feature identity.

Supplementary Materials: The following supporting information can be downloaded at: https://www.mdpi.com/article/10.3390/jmse14212004/s1. The monthly AZMP SSF dataset for 1993–2017 and the Peak SSF dataset for 1993–2025 are provided as separate comma-separated values (CSV) files.

Author Contributions: Conceptualization, S.S.; methodology, S.S., F.R. and B.G.; formal analysis, S.S., F.R. and B.G.; data curation, B.G.; writing—original draft preparation, S.S.; writing—review and editing, S.S., F.R. and B.G.; funding acquisition, S.S. All authors have read and agreed to the published version of the manuscript.

Funding: This research was funded by the CDARP program at RMC.

Data Availability Statement: The monthly AZMP SSF and Peak SSF datasets analyzed in this study are provided in the Supplementary Materials. ARMOR3D data are available from the Copernicus Marine Service [28], and GEBCO 2026 bathymetry is available from the GEBCO Compilation Group [29].

Acknowledgments: This work builds on historical SSF position datasets developed at Fisheries and Oceans Canada and maintained through the Atlantic Zone Monitoring Program. We thank the analysts and data curators who sustained the monthly dataset [11], as well as the research support that enabled this study. S.S. acknowledges sabbatical support at RMC and the Bedford Institute of Oceanography and assistance from the BIO Library in locating historical Gulf Stream mapping materials. We remember the late Keith R. Thompson. This study grew in part from discussions with Keith and from the demonstration by Thompson and Demirov [36] that sea-level skewness can delineate the Gulf Stream path and distinguish cyclonic from anticyclonic variability. It was also informed by the regional modeling of the Gulf of Maine, Scotian Shelf, and adjacent deep ocean developed by Keith's group. We thank Lequan Chi for sharing his insight on the Shelf-Slope Front and the Gulf Stream North Wall during the early stages of the study. We thank Charles Hannah and Zeliang Wang for helpful discussions. We also thank the three anonymous reviewers for their

constructive comments and suggestions, which helped improve the presentation and clarity of the manuscript.

Conflicts of Interest: The authors declare no conflicts of interest.

References

1. Belkin, I.M.; Cornillon, P.C.; Sherman, K. Fronts in large marine ecosystems. *Prog. Oceanogr.* **2009**, *81*, 223–236. [CrossRef]
2. Brink, K.H. Cross-shelf exchange. *Annu. Rev. Mar. Sci.* **2016**, *8*, 59–78. [CrossRef] [PubMed]
3. Beardsley, R.C.; Flagg, C.N. The water structure, mean currents, and shelf water/slope water front of the New England continental shelf. *Proc. 1975 Liège Colloq. Hydrodyn.* **1976**, *10*, 209–225.
4. Bisagni, J.J.; Kim, H.-S.; Drinkwater, K.F. Observations and modeling of shelf-slope front seasonal variability between 75° and 50°W. *Deep.-Sea Res. Part II Top. Stud. Oceanogr.* **2006**, *53*, 2477–2500. [CrossRef]
5. Csanady, G.T.; Hamilton, P. Circulation of slopewater. *Cont. Shelf Res.* **1988**, *8*, 565–624. [CrossRef]
6. Gatien, M.G. A study in the Slope Water region south of Halifax. *J. Fish. Res. Board Can.* **1976**, *33*, 2213–2217. [CrossRef]
7. Hinrichsen, H.-H.; Tomczak, M. Optimum multiparameter analysis of the water mass structure in the western North Atlantic Ocean. *J. Geophys. Res. Oceans* **1993**, *98*, 10155–10169. [CrossRef]
8. Houghton, R.W.; Smith, P.C.; Fournier, R.O. A simple model for cross-shelf mixing on the Scotian Shelf. *J. Fish. Res. Board Can.* **1978**, *35*, 414–421. [CrossRef]
9. Gawarkiewicz, G.; Ferdelman, T.G.; Church, T.M.; Luther, G.W., III. Shelfbreak frontal structure on the continental shelf north of Cape Hatteras. *Cont. Shelf Res.* **1996**, *16*, 1751–1773. [CrossRef]
10. Chamberlin, J.L. Application of satellite infrared data to analysis of ocean frontal movements and water mass interactions off northeastern United States. *NAFO Sci. Counc. Stud.* **1982**, *4*, 21–30.
11. Drinkwater, K.F.; Myers, R.A.; Pettipas, R.G.; Wright, T.L. Climatic data for the northwest Atlantic: The position of the shelf/slope front and the northern boundary of the Gulf Stream between 50°W and 75°W, 1973-1992. *Can. Data Rep. Hydrogr. Ocean Sci.* **1994**, *125*, 1–103.
12. Drinkwater, K.F.; Bugden, G.L. *Variability in the position of the shelf/slope front near the mouth of the Laurentian Channel*; DFO Atlantic Fisheries Research Document 94/10; Department of Fisheries and Oceans Canada: Dartmouth, NS, Canada, 1994.
13. Peterson, I.; Greenan, B.; Gilbert, D.; Hebert, D. Variability and wind forcing of ocean temperature and thermal fronts in the slope water region of the Northwest Atlantic. *J. Geophys. Res. Oceans* **2017**, *122*, 7325–7343. [CrossRef]
14. Cayula, J.-F.; Cornillon, P.C. Edge detection algorithm for SST images. *J. Atmos. Ocean. Technol.* **1992**, *9*, 67–80. [CrossRef]
15. Ullman, D.S.; Cornillon, P.C. Satellite-derived sea surface temperature fronts on the continental shelf off the northeast U.S. coast. *J. Geophys. Res. Oceans* **1999**, *104*, 23459–23478. [CrossRef]
16. Belkin, I.M.; O'Reilly, J.E. An algorithm for oceanic front detection in chlorophyll and SST satellite imagery. *J. Mar. Syst.* **2009**, *78*, 319–326. [CrossRef]
17. Cyr, F.; Larouche, P. Thermal fronts atlas of Canadian coastal waters. *Atmos.-Ocean* **2015**, *53*, 212–236. [CrossRef]
18. Shaw, A.G.P.; Vennell, R. A front-following algorithm for AVHRR SST imagery. *Remote Sens. Environ.* **2000**, *72*, 317–327. [CrossRef]
19. Hopkins, J.; Challenor, P.; Shaw, A.G.P. A new statistical modeling approach to ocean front detection from SST satellite images. *J. Atmos. Ocean. Technol.* **2010**, *27*, 173–191. [CrossRef]
20. Ullman, D.S.; Cornillon, P.C. Evaluation of front detection methods for satellite-derived SST data using in situ observations. *J. Atmos. Ocean. Technol.* **2000**, *17*, 1667–1675. [CrossRef]
21. Bisagni, J.J.; Nichols, O.C.; Pettipas, R. Interannual variability of Gulf Stream warm-core ring interactions with the outer continental shelf and potential broad scale relationships with longfin squid (*Doryteuthis pealeii*) relative abundance, 1981–2004. *ICES J. Mar. Sci.* **2019**, *76*, 1257–1270. [CrossRef]
22. Watelet, S.; Beckers, J.-M.; Barth, A. Reconstruction of the Gulf Stream from 1940 to the present and correlation with the North Atlantic Oscillation. *J. Phys. Oceanogr.* **2017**, *47*, 2741–2754. [CrossRef]
23. Chi, L.; Hameed, S.; Wolfe, C.L.P. Comments on "Reconstruction of the Gulf Stream from 1940 to the present and correlation with the North Atlantic Oscillation". *J. Phys. Oceanogr.* **2019**, *49*, 2731–2734. [CrossRef]
24. Chi, L.; Wolfe, C.L.P.; Hameed, S. The distinction between the Gulf Stream and its North Wall. *Geophys. Res. Lett.* **2019**, *46*, 8943–8951. [CrossRef]
25. McWilliams, J.C.; Gula, J.; Molemaker, M.J. The Gulf Stream North Wall: Ageostrophic circulation and frontogenesis. *J. Phys. Oceanogr.* **2019**, *49*, 893–916. [CrossRef]
26. Guinehut, S.; Dhomps, A.-L.; Larnicol, G.; Le Traon, P.-Y. High resolution 3-D temperature and salinity fields derived from in situ and satellite observations. *Ocean Sci.* **2012**, *8*, 845–857. [CrossRef]
27. Mulet, S.; Rio, M.-H.; Mignot, A.; Guinehut, S.; Morrow, R. A new estimate of the global 3D geostrophic ocean circulation based on satellite data and in situ measurements. *Deep.-Sea Res. Part II Top. Stud. Oceanogr.* **2012**, *77–80*, 70–81. [CrossRef]

28. Copernicus Marine Service. Multi Observation Global Ocean 3D Temperature Salinity Height Geostrophic Current and MLD (ARMOR3D) [Data Set]. 2025. Available online: https://data.destination-earth.eu/data-portfolio/EO.MO.DAT.MULTIOBS_GLO_PHY_TSUV_3D_MYNRT_015_012 (accessed on 25 March 2026). [CrossRef]
29. GEBCO Bathymetric Compilation Group. The GEBCO_2026 Grid-A Continuous Terrain Model for Oceans and Land at 15 Arc-Second Intervals [Data Set]. NERC EDS British Oceanographic Data Centre NOC. 2026. Available online: https://catalogue.ceda.ac.uk/uuid/fb236c93aa574cb9b5154db45dfdd784/ (accessed on 30 September 2026). [CrossRef]
30. Huber, P.J.; Ronchetti, E.M. *Robust Statistics*; John Wiley & Sons: New York, NY, USA, 1981.
31. Dupont, F.; Hannah, C.G.; Wright, D.G. Model investigation of the Slope Water, north of the Gulf Stream. *Geophys. Res. Lett.* **2006**, *33*, L05604. [CrossRef]
32. Shan, S.; Sheng, J.; Greenan, B.J.W. Physical processes affecting circulation and hydrography in the Sable Gully of Nova Scotia. *Deep.-Sea Res. Part II Top. Stud. Oceanogr.* **2014**, *104*, 35–50. [CrossRef]
33. Wang, Z.; Yang, J.; Johnson, C.; DeTracey, B. Changes in deep ocean contribute to a 'see-sawing' Gulf Stream path. *Geophys. Res. Lett.* **2022**, *49*, e2022GL100937. [CrossRef]
34. Paquin, J.-P.; Roy, F.; Smith, G.C.; MacDermid, S.; Lei, J.; Dupont, F.; Lu, Y.; Taylor, S.; St-Onge-Drouin, S.; Blanken, H.; et al. A new high-resolution Coastal Ice-Ocean Prediction System for the East Coast of Canada. *Ocean Dyn.* **2024**, *74*, 799–826. [CrossRef]
35. Ohashi, K.; Laurent, A.; Renkl, C.; Sheng, J.; Fennel, K.; Oliver, E. DalROMS-NWA12 v1.0, a coupled circulation-ice-biogeochemistry modelling system for the northwest Atlantic Ocean: Development and validation. *Geosci. Model Dev.* **2024**, *17*, 8697–8733. [CrossRef]
36. Thompson, K.R.; Demirov, E. Skewness of sea level variability of the world's oceans. *J. Geophys. Res. Oceans* **2006**, *111*, C05005. [CrossRef]
37. Béguer-Pon, M.; Castonguay, M.; Shan, S.; Benchetrit, J.; Dodson, J.J. Direct observations of American eels migrating across the continental shelf to the Sargasso Sea. *Nat. Commun.* **2015**, *6*, 8705. [CrossRef] [PubMed]
38. Zhang, W.G.; Partida, J. Frontal subduction of the Mid-Atlantic Bight shelf water at the onshore edge of a warm-core ring. *J. Geophys. Res. Oceans* **2018**, *123*, 7795–7818. [CrossRef]
39. Chen, K.; Gawarkiewicz, G.; Yang, J. Mesoscale and submesoscale shelf-ocean exchanges initialize an advective marine heatwave. *J. Geophys. Res. Oceans* **2022**, *127*, e2021JC017927. [CrossRef]
40. Burges, C.J.C.; Shaked, T.; Renshaw, E.; Lazier, A.; Deeds, M.; Hamilton, N.; Hullender, G.N. Learning to rank using gradient descent. In Proceedings of the 22nd International Conference on Machine Learning, Bonn, Germany, 7–11 August 2005; pp. 89–96. [CrossRef]
41. Roberts, D.R.; Bahn, V.; Ciuti, S.; Boyce, M.S.; Elith, J.; Guillera-Arroita, G.; Hauenstein, S.; Lahoz-Monfort, J.J.; Schroder, B.; Thuiller, W.; et al. Cross-validation strategies for data with temporal, spatial, hierarchical, or phylogenetic structure. *Ecography* **2017**, *40*, 913–929. [CrossRef]
42. Ronneberger, O.; Fischer, P.; Brox, T. U-Net: Convolutional networks for biomedical image segmentation. In *Medical Image Computing and Computer-Assisted Intervention—MICCAI 2015*; Navab, N., Hornegger, J., Wells, W.M., Frangi, A.F., Eds.; Lecture Notes in Computer Science; Springer: Cham, Switzerland, 2015; Volume 9351, pp. 234–241. [CrossRef]

Disclaimer/Publisher's Note: The statements, opinions and data contained in all publications are solely those of the individual author(s) and contributor(s) and not of MDPI and/or the editor(s). MDPI and/or the editor(s) disclaim responsibility for any injury to people or property resulting from any ideas, methods, instructions or products referred to in the content.